Microstructural Engineering of Hydroxyapatite Membranes to Enhance Proton Conductivity

By *Dongxia Liu, Keith Savino,* and *Matthew Z. Yates**

A new approach to enhancing proton conductivity of ceramics is demonstrated by aligning proton conductive pathways and eliminating resistive grain boundaries. Hydroxyapatite (HAP) membranes are synthesized by multistage crystallization onto palladium. The synthesis involves three steps: electrochemical deposition of HAP seeds, secondary hydrothermal crystallization onto the seed layer to promote *c*-axis growth normal to the substrate, and tertiary hydrothermal crystallization to promote *a*-axis growth to fill the gaps between the aligned crystals. The *c*-axis alignment with crystal domains spanning the membrane thickness significantly enhances proton conduction since protons are primarily transported along the *c*-axes of HAP crystals. The novel HAP membranes display proton conductivity almost four orders of magnitude higher than traditional sintered HAP ceramics. The HAP membranes on palladium hydrogen membrane substrates hold promise for use in intermediate-temperature fuel cells, chemical sensors, and other devices. The synthesis approach presented may also be applied to other ion-conducting membrane materials to enhance transport properties.

1. Introduction

The development of high-performance ion-conducting membranes is crucial to the commercialization of fuel cell devices that provide clean electrical power generation from renewable fuel sources.[1–3] The two classes of fuel cells under most intensive research and development are polymer electrolyte membrane fuel cells (PEMFCs) and solid oxide fuel cells (SOFCs). Dehydration and chemical instability of polymer electrolytes limit the operating temperature of PEMFCs to about 115 °C.[4,5] At these relatively low temperatures, a high loading of precious metal catalysts is needed on both the anode and cathode of the fuel cell to enable fast reaction kinetics. In addition, expensive and energy-intensive fuel processing is required to remove traces of carbon monoxide that poison PEMFC catalysts under typical operating conditions. SOFCs are capable of stable operation at much higher temperatures, allowing the use of inexpensive nonprecious metal catalysts due to favorable reaction kinetics. SOFCs also may be fueled directly on reformed hydrogen gas because the catalysts are insensitive to carbon monoxide impurity.[1] The drawback of SOFCs is the very high operating temperatures, typically above 800 °C, which are required for sufficient ion conductivity in typical ceramic membranes.[6] The high operating temperature forces the construction of SOFC components out of expensive high-temperature ceramics, and can cause device failure due to thermal stress upon temperature cycling from ambient to operating conditions.[7,8]

Fuel cells operating in the intermediate temperature range of 200–700 °C are promising for reducing cost and enhancing performance. The intermediate temperature range is low enough to allow fuel cell construction from inexpensive materials, but high enough to use nonprecious metal catalysts and allow internal fuel reforming of hydrocarbon fuels. Although intermediate-temperature fuel cells are under intense research at present time, few materials have sufficiently high ionic conductivity in the desired temperature range.[2] Development of intermediate-temperature fuel cells has focused on either creating new membrane materials with higher conductivity, or making existing membranes thinner to reduce overall resistance to ion transport.[9,10] Here we report a different approach for improving the performance of ion-conducting membranes by engineering the membrane microstructure to optimize ion transport. Our approach is analogous to the microstructural optimization of zeolite and molecular sieve membranes to improve mass transport.[11,12]

Microstructural engineering was carried out to create proton conducting hydroxyapatite (HAP) membranes. HAP is a type of calcium phosphate crystal with a hexagonal crystallographic structure and a stoichiometric Ca/P molar ratio of 1.67.[13,14] The proton conductivity in HAP ceramics at elevated temperatures has been attributed to the migration of protons along hydroxyl groups lining the *c*-axis of the crystal domains.[15,16] Grain boundaries between crystal domains have been shown to act as traps for proton transport.[17] High-temperature polarization/depolarization studies confirm proton transport along the *c*-axis and show an onset of proton mobility at temperatures as low as 200–250 °C.[16] It is therefore expected that the optimal proton conductivity would occur when the *c*-axes of crystal domains are aligned and span the

---

[*] Prof. M. Z. Yates, D. Liu, K. Savino
Department of Chemical Engineering and
Laboratory for Laser Energetics
University of Rochester
Rochester, NY, 14627 (USA)
E-mail: myates@che.rochester.edu

DOI: 10.1002/adfm.200900318

thickness of the HAP membrane. In that way, grain boundary resistance would be eliminated, and the transport path optimized. Such microstructurally optimized HAP membranes are expected to have significantly higher proton conductivity, allowing proton transport at lower temperatures than would otherwise be effective.

Electrochemical deposition has been widely studied for coating HAP on titanium, stainless steel, and titanium alloy substrates for bioactive surface modification for orthopedic implants.[18–20] An electric current is applied through an aqueous solution near neutral pH containing dissolved Ca^{2+} and $HPO_4{}^{2-}$. The applied electric current causes a local increase in pH near the cathode due to electrolysis of water and accumulation of Ca^{2+} near the cathode due to electrostatic attraction. As a result, calcium phosphate becomes locally supersaturated and HAP crystals nucleate and grow on the cathode surface. The crystals tend to grow with *c*-axes oriented normal to the cathode surface since the *c*-axis is the fastest growing.[12,21]

Previous investigations have shown that at elevated temperatures in a hydrogen atmosphere, palladium electrodes inject protons into HAP ceramics.[15] The palladium serves as a hydrogen membrane at elevated temperatures, with hydrogen dissolving in the palladium in the form of protons and electrons. The protons can travel through the palladium electrode and into HAP. When a proton conductor and cathode catalyst layer are deposited onto a palladium membrane, a "hydrogen membrane fuel cell" (HMFC) can be created.[22] Very thin, fragile proton conducting layers can be used in an HMFC because they are supported by the palladium. As a result, performance in the intermediate temperature range is enhanced. A previous study has shown excellent performance of an HMFC in the 300–600 °C temperature range using a thin proton conducting layer deposited by pulsed laser vapor deposition.[22] In the present study, electrochemical deposition was used to deposit an ultrathin HAP seed crystal layer directly onto a palladium surface.

HAP seed layers deposited electrochemically onto palladium were converted to thin membranes through a novel multistep synthesis. First, hydrothermal crystallization was carried out to promote growth of crystals onto the seed layer with the *c*-axes preferentially oriented normal to the surface. Next, a second hydrothermal crystallization step was conducted under conditions that promote *a*-axis growth. The *a*-axis growth causes intergrowth of crystals into a dense film. The result is a continuous membrane with crystal domains aligned for enhanced proton transport.

2. Results and Discussion

A typical recipe of electrochemical/hydrothermal synthesis of HAP films on titanium substrates is under constant current conditions of ~12.5 mA cm^{-2} at temperatures of 100–200 °C for a period of ~1 h.[18] Unfortunately, under these typical synthesis conditions, palladium is destroyed due to hydrogen embrittlement that occurs when pure palladium is exposed to hydrogen at temperatures below 293 °C.[23] Since hydrogen gas is evolved at the cathode during electrolysis and HAP grows only on the cathode, the HAP cannot be electrochemically deposited without exposing the palladium membrane directly to hydrogen gas. It was found that reducing the amount of hydrogen produced during the experiment by applying a smaller electrical current (typically less than 10 mA cm^{-2}) and/or a shorter deposition time (less than 5 min) allowed an ultrathin HAP seed layer to be produced without damaging the palladium substrate. As an example, Figure 1a–b shows a HAP layer that forms on the palladium substrate in 4 min at 95 °C using a constant current density of 9.5 mA cm^{-2}. The HAP crystals have platelet morphology with a length of 1~2 μm and a submicrometer width, as shown in Figure 1a. Figure 1b indicates that the crystals are preferentially oriented normal to the palladium substrate. The X-ray diffraction (XRD) pattern in Figure 2a identifies the crystals as HAP, formed most likely from platelike octacalcium phosphate, a crystal phase that appears usually at low pH and certain temperature ranges in the electrochemical deposition of HAP.[24] For randomly oriented HAP crystals, the intensity of the (002) plane diffraction peak is small compared to that of the (300) plane, as shown in Figure 2d. The enhanced diffraction from the (002) plane observed in Figure 2a indicates a [002] (i.e., *c*-axis) preferred orientation normal to the palladium substrate.

To promote growth of a dense HAP membrane, the electrochemically deposited crystals were used as seeds for secondary crystallization onto the palladium surface. The secondary crystallization was carried out under hydrothermal conditions known to produce large sized HAP crystals with excellent crystal quality.[25–27] A calcium chelating agent, ethylenediamine tetraacetic acid (EDTA), was used to control supersaturation of HAP and thus adjust the crystal growth rate. It is known that crystals tend to grow from seeded surfaces with the fastest growing axis (in this case, the

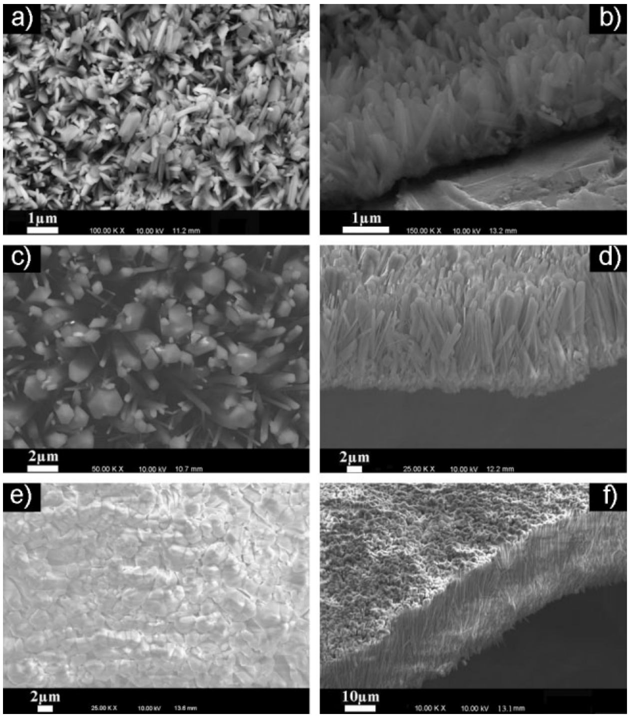

Figure 1. Morphology and microstructure of HAP membranes grown on palladium substrate: a) top-view and b) side-view of HAP seed layer prepared by electrochemical deposition at 9.5 mA cm^{-2} current in 4 min; c) top-view and d) side-view of HAP film after secondary hydrothermal growth at 200 °C for 15 h; e) top-view and f) side-view of HAP film after tertiary hydrothermal growth at 200 °C for 60 h.

c-axis) normal to the surface.[12,21] Figure 1c–d shows the surface morphology and cross-sectional morphology of the HAP crystal layer grown after secondary hydrothermal crystallization. Most crystals are rod-shaped, having a well-defined hexagonal crystal habit with a width up to ~2 μm (Fig. 1c). The rod-shaped crystals are oriented perpendicular all the way down to the substrate with a length of ~7 μm (Fig. 1d). The XRD pattern of the HAP film (Fig. 2b) shows a strong enhancement in intensity of (002) diffraction peak. The enhanced (002) reflection indicates that the *c*-axes of HAP crystals are oriented normal to the palladium substrate, consistent with the scanning electron microscopy (SEM) observation in Figure 1d.

Secondary hydrothermal growth onto the seed layer resulted in highly *c*-axis aligned rodlike crystals, but did not result in dense HAP films. One route to create dense HAP films is through a tertiary crystallization step that promotes *a*-axis growth rather than *c*-axis growth. A similar approach has been employed on molecular sieve films to promote lateral intergrowth of crystals to create continuous membranes for chemical separations.[12] A number of researchers have employed molecular additives called crystal growth modifiers to engineer crystal morphology.[28–30] Crystal growth modifiers function by adsorbing preferentially onto a specific crystal face through electrostatic attraction or other intermolecular interaction to slow growth on that face. As a result, the relative growth on other faces is faster and the crystal shape changes. Studies of HAP as a liquid chromatography packing indicate that HAP crystals have positively charged *a*-surfaces and negatively charged *c*-surfaces.[14] Therefore, it is expected that cationic additives may function as crystal growth modifiers for HAP to slow growth on the *c*-axis and thus promote *a*-axis growth. To test this hypothesis, the cationic surfactant cetylpyridinium chloride was investigated as a crystal growth modifier in tertiary crystallization HAP.

It was found that cetylpyridinium chloride promotes the lateral intergrowth of HAP crystals during tertiary hydrothermal crystallization and results in a dense and strongly adherent layer on the substrate. Figure 1e–f shows the morphology of a HAP film after 60 h of tertiary hydrothermal growth. The starting substrate was a film produced by secondary growth similar to that shown in Figure 1c–d. The top-view of the film shows that the crystal domains grow together, although some small gaps remain. The small gaps do not extend completely through the membrane, as visualized in the side-view image. The crystal domains in the film are oriented normal to the palladium substrate with a thickness of approximately 25 μm. The crystals in the film appear larger both in width and length than those after secondary growth, which means HAP crystallization occurs along not only the *a*-axis direction, but also the *c*-axis direction in the tertiary crystallization. However, the rate of crystal growth along the *a*-axis appears enhanced relative to that in secondary crystallization, since the crystals grow together into a dense film in the tertiary step. The crystal *c*-axis orientation was further verified with XRD characterization, as shown in Figure 2c. The XRD pattern has a strong peak corresponding to the (002) reflection plane and all other peaks are suppressed. The XRD pattern shows nearly ideal alignment of the HAP crystal domains in the membrane after tertiary growth.

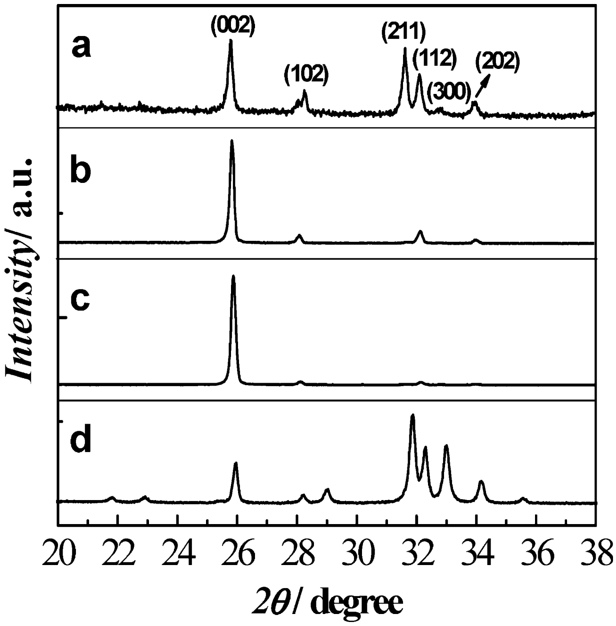

Figure 2. XRD of HAP seeds (a), HAP film on the palladium substrate after secondary hydrothermal growth (b), and HAP film after tertiary hydrothermal growth (c) on palladium substrate. The XRD pattern of randomly distributed HAP crystals collected from the tertiary hydrothermal growth (d).

In a control experiment, 60 h of hydrothermal crystallization was carried out on a clean palladium substrate. The results showed that without the HAP seed layer, very little crystallization occurred onto the surface and the crystals were not oriented normal to the substrate, as shown in Figure 3. To confirm the role of cetylpyridinium chloride as a crystal growth modifier, another control experiment was carried out under the same conditions as those of HAP dense membrane formation except for the addition of cetylpyridinium chloride. Electron microscopy images from the control experiment show that individual crystals in the film grew longer than 25 μm, but many gaps between crystals still exist and extend down to the bottom of the film, as shown in Figure 4. The results of the control experiment confirm that without cetylpyridinium chloride, the growth rate of the *a*-axis is reduced.

The elemental composition and calcium-to-phosphorous (Ca/P) atomic ratio of the HAP membranes were studied with

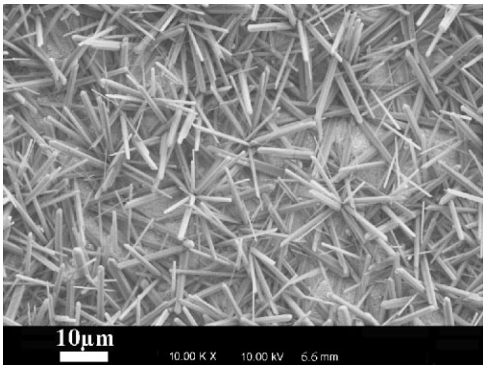

Figure 3. Morphology of HAP on palladium substrate without seed layer after hydrothermal crystal growth at 200 °C for 60 h.

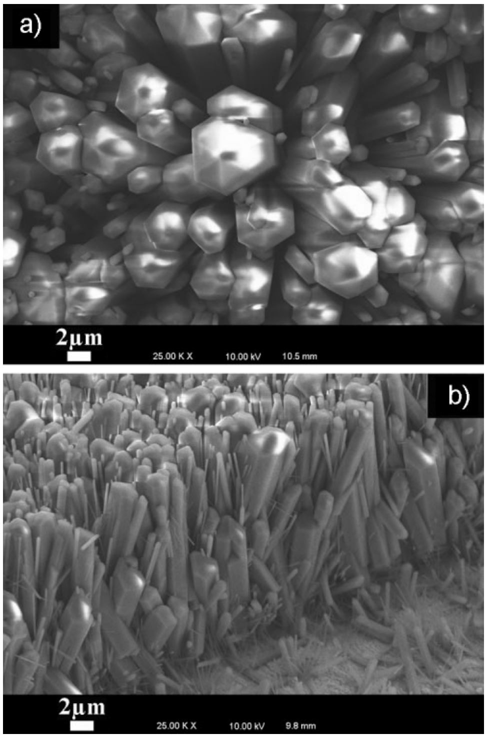

Figure 4. a) Top-view and b) side-view morphology of HAP on palladium substrate after tertiary hydrothermal growth at 200 °C for 60 h in the absence of cetylpyridinium chloride.

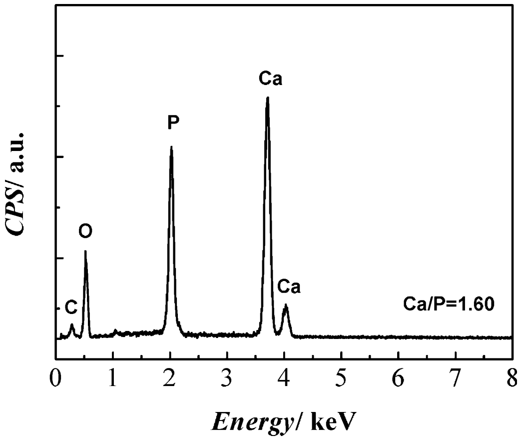

Figure 5. EDX spectrum of HAP film on palladium substrate after tertiary hydrothermal growth.

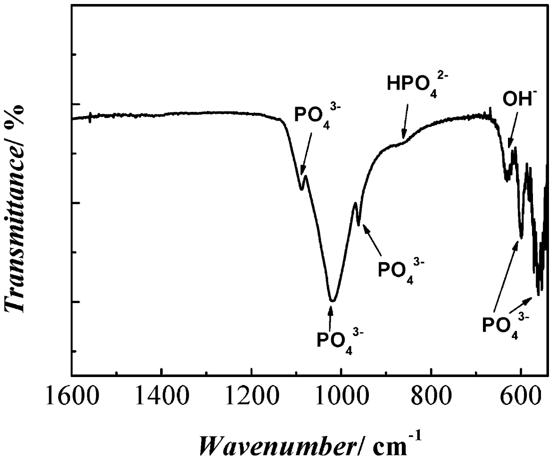

Figure 6. FTIR spectrum of HAP membrane on palladium substrate after tertiary hydrothermal growth.

an energy dispersive X-ray (EDX) spectrometer. The EDX spectrum (Fig. 5) comprises O, P and Ca peaks, confirming the presence of HAP. The C peak is more likely from the carbon tape used for the SEM observation. The semiquantitative analysis of the EDX spectrum shows the Ca/P atomic ratio is around 1.60, a little lower than the ideal stoichiometric value of 1.67. The nonstoichimetry (Ca deficiency) of HAP is consistent with reports from the literature for hydrothermal synthesis of HAP crystals.[26,27] The Fourier transform IR (FTIR) spectrum of HAP membranes in Figure 6 shows all PO_4^{3-} and OH^- absorption bands characteristic for HAP.[26,31] For PO_4^{3-} groups, the ν_1 vibration (symmetric stretching) centers at 961 cm^{-1}, ν_3 vibration (asymmetric stretching) occurs at 1088 and 1022 cm^{-1}, while ν_4 vibration (asymmetric bending) locates at 602, 580, and 562 cm^{-1}. The librational vibration of OH^- groups appears at 631 cm^{-1}. Absence of any distinct bands in the range of 1400–1500 cm^{-1} indicates that HAP does not contain large quantities of carbonate ions. The band observed at 870 cm^{-1} is ascribed to the HPO_4^{2-} groups, in agreement with data reported in the literature.[26,31] The presence of HPO_4^{2-} groups is consistent with the low Ca/P atomic ratio in the synthesized HAP crystalline films.

For ion-conducting membranes in fuel cells, it is desirable to not only create materials with the highest possible conductivity, but also to make the thinnest possible gas-tight membrane to reduce the overall resistance to ion transport. The thickness of the HAP membranes shown in Figure 1e–f is around 25 μm. A series of experiments were performed in order to find conditions that would yield a dense film with desirable smaller thickness. The results show that the membrane thickness can be reduced by using a shorter electrochemical deposition time for the seed layer and higher molar ratio of calcium to phosphate (or, lower phosphate concentration) in the hydrothermal secondary and tertiary crystallization steps. Reducing the electrochemical deposition time resulted in a thinner seed layer, as shown in Figure 7a–b. The seed layer was only around 300 and 600 nm thick when the electrochemical deposition time was 1 and 2 min, respectively. In comparison, the seed layer is ~1–2 μm thick when the deposition time was 4 min, as shown in Figure 1b. Secondary and tertiary hydrothermal crystallization was carried out on the two seeded surfaces shown in Figure 3a–b. The synthetic conditions were the same as used to grow the ~25 μm thick film shown in Figure 1f except the phosphate concentration was reduced from 0.06 to 0.01 M. After the reaction, the films synthesized from the ~600 and ~300 nm seed layers were ~5 and ~2.5 μm thick, respectively, as shown in Figure 7c–d. The reduced film thickness is partially due to the thin seed layers produced in the electrochemical deposition. The reduced phosphate concentration also alters crystal growth, possibly by controlling the degree of supersaturation.[32] A more detailed and systematic study should be conducted to determine

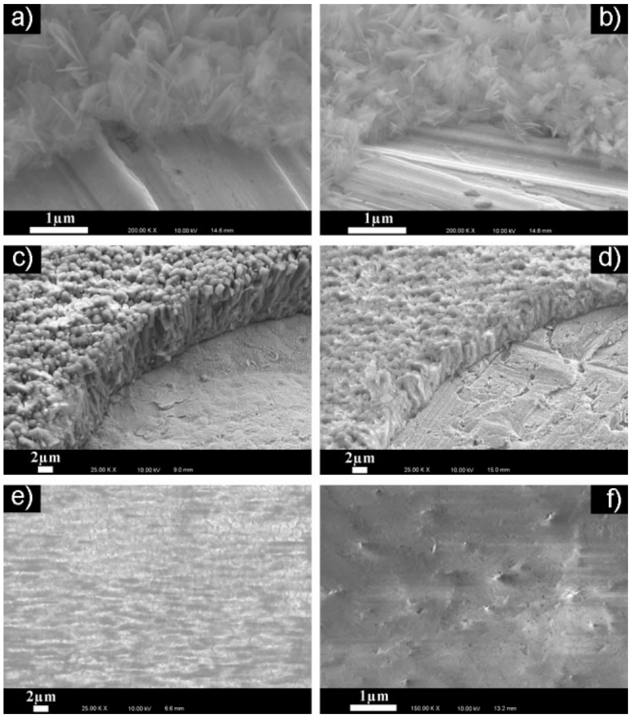

Figure 7. a,b) SEM images of HAP seed layers on palladium substrate prepared by electrochemical deposition at 9.5 mA cm^{-2} current density in 2 (a) and 1 (b) min; c,d) the morphology of HAP membranes after tertiary hydrothermal synthesis grown from the seed layer in (a) and (b), respectively; e,f) top and bottom surfaces of the HAP membrane in (d).

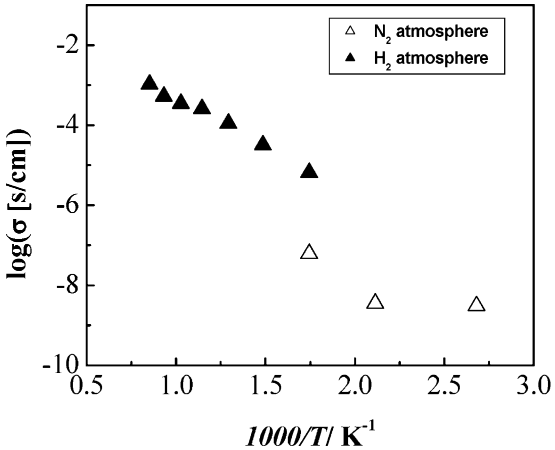

Figure 8. Proton conductivity of the HAP thin membranes on palladium substrate prepared by the seeded hydrothermal growth processes.

the crystal growth mechanism under varied hydrothermal conditions. The ~2.5 µm HAP thin films still have a dense and continuous morphology, as shown in Figure 7e–f. The top surface in Figure 7e shows crystal domains grown together into a dense film. The bottom surface is smooth and dense (Fig. 7f). The few small protrusions in the bottom surface are a result of the palladium substrate not being perfectly flat and smooth. The results are encouraging that thin gas-tight coatings of HAP may be synthesized that would be suitable for fuel cell membranes or other applications.

Electrical impedance spectroscopy was carried out to characterize the proton conductivity of the films. The measurement was conducted on a HAP film ~25 µm thick, similar to that shown in Figure 1e–f created after tertiary crystallization. Figure 8 shows the resulting proton conductivity as a function of temperature up to 900 °C. In the measurement, the palladium layer was sealed on a ceramic tube with the HAP layer facing outward. The HAP layer was exposed to dry air, while nitrogen was fed to the palladium side as it was heated. At 100–200 °C, the measured conductivity was very low, ~10^{-9} S cm^{-1}. At 300 °C, the conductivity was ~10^{-7} S cm^{-1} when nitrogen was being fed into the tube. The conductivity jumped to ~10^{-5} S cm^{-1} at 300 °C after switching from nitrogen to hydrogen flow to the palladium side. The enhancement of proton conductivity at 300 °C when exposing the membrane to hydrogen atmosphere is due to the injection of protons into the HAP thin films from palladium.[15] The injected protons increase the number of transporting protons in the crystalline membrane, and as a result, enhance the membrane proton conductivity. The conductivity increased steadily with temperature above 300 °C, reaching ~10^{-3} S cm^{-1} at 800 °C with hydrogen on the palladium side. In comparison, a traditional sintered HAP ceramic in dry air at 800 °C has a conductivity of ~5 × 10^{-7} S cm^{-1}, nearly four orders of magnitude lower.[33] A control experiment measuring the proton conductivity of a traditional sintered HAP pellet under flowing hydrogen showed a conductivity of ~7 × 10^{-6} S cm^{-1} (see Supplementary Information), which is still much lower than that of the microstructurally engineered HAP membranes. A calculation based on the Arrhenius equation yields an activation energy of proton conduction in the microstructurally engineered HAP membrane of 0.49 eV, which is lower than that of HAP materials reported in literature.[13,15,17] The activation energy is similar to that of other proton conducting ceramics investigated for fuel cell use.[34,35] The conductivity value of 10^{-3} S cm^{-1} is similar to the proton conductivity of yttrium-substituted BaCeO$_3$ at 800 °C in dry air,[36,37] but lower than the oxide ion conductivity of YSZ-based (YSZ = yttria-stabilized zirconia) electrolytes at the same temperature.[6] Thin yttrium-substituted BaCeO$_3$ membranes deposited by pulsed laser deposition have already shown to give excellent performance in hydrogen membrane fuel cells. The conductivity results suggest that the HAP membrane with aligned crystal domains may be capable of giving similar fuel cell performance. It should be noted that interfacial resistance between the electrodes and HAP may give a non-negligible contribution to the overall measured resistance because the film thickness is small (~25 µm). Therefore, the actual proton conductivity may be higher than that measured in Figure 8.

To examine the stability of the HAP membrane to water vapor, the membrane was placed in a sealed vessel containing saturated water vapor at 170 °C for 48 h, following a procedure reported in the literature.[38] According to the Clasius–Clapeyron equation, the partial pressure of water at this condition is 11.5 atm. The partial pressure is higher than the membrane would encounter in an operating fuel cell based on this proton conducting membrane. The HAP membranes are stable under the examined condition, as confirmed by SEM, XRD, and FTIR analysis, respectively. The

SEM, XRD, and FTIR results show no measurable change compared to those measured before the stability test. The high stability of the HAP membranes to water vapor indicates potential application of HAP as electrolyte in intermediate temperature fuel cells.

3. Conclusions

In conclusion, the synthetic process developed shows a route to significantly enhance proton transport by aligning proton conductive pathways and eliminating grain boundary resistance. The synthetic approach to enhance ion transport is analogous to that used on molecular sieve and zeolite membranes to enhance mass transport. By adjusting synthetic conditions, the film can be grown into different thicknesses with a dense coverage on the underlying substrate. Proton conductivity measurement demonstrates significant enhancement of proton conductivity compared to traditional sintered HAP. The *c*-axis aligned HAP films are very promising for integration into fuel cells in the intermediate temperature range. The microstructural engineering by multistage crystallization presented here can potentially be applied to create other ion-conducting materials with optimized properties, useful for separations and catalysis as well as electronic and electrochemical applications, electrochemical membrane reactors, and in chemical sensors.

4. Experimental

Materials: Analytic grade $Ca(NO_3)_2 \cdot 4H_2O$ (99.0% purity) and $(NH_4)_2HPO_4$ (>99.0% purity) were purchased from Alfa Aesar and EMD, respectively. Disodium ethylenediaminetetraacetate dehydrate ($Na_2EDTA \cdot 2H_2O$) (ACS reagent, 99.0–101.0% purity) and cetylpyridinium chloride monohydrate (99.0–101.0% purity) were obtained from Sigma-Aldrich. Pure 28.0–30.0% ammonium hydroxide was purchased from Mallinckrodt Chemicals. Sintered porous 316L stainless steel discs (0.2 μm pore size, 1.60 mm thick, and 12.7 mm diameter) were obtained from Small Parts, Inc. Deionized water was used throughout the experiments.

Preparation of HAP Seeds on Palladium Substrates: Palladium substrates were prepared by electroless plating of a thin layer of palladium onto porous stainless steel supports following a reported procedure [39,40]. Typically, the plated palladium layer was around 20 μm thick, which was enough to seal the pores at the surface of the substrates. HAP seeds were deposited via electrochemical deposition using palladium as the cathode. The anode was a platinum plate (25 mm × 25 mm × 127 μm). The anode and cathode electrodes were arranged parallel and held 10 mm apart in an electrolyte solution prepared as described in the literature [18,19]. The electrochemical reaction was carried out at 95 °C for a desired time with a constant direct current. After the deposition, the palladium electrode was taken out of the solution, rinsed with deionized water, and dried in air.

Secondary Growth of HAP: The seeded palladium substrate was placed in a Teflon-lined vessel with the seed layer facing down and tilted up ~45° relative to the bottom of the vessel. A solution of Na_2EDTA (0.20 M) and $Ca(NO_3)_2$ (0.20 M) was prepared in deionized water (15 mL). A solution of $(NH_4)_2HPO_4$ (0.12 M) in deionized water (15 mL) was prepared in a second container. The two source solutions were mixed together after pH of each solution was raised to 10.0 with ammonium hydroxide. The resulting combined solution was transferred to the Teflon-lined vessel sealed in a stainless steel autoclave. The hydrothermal synthesis was carried out in an oven for 15 h at 200 °C. After the reaction, the sample was rinsed with deionized water and dried in air.

Tertiary Growth of HAP: The synthetic solution was prepared by dissolving Na_2EDTA (0.20 M), $Ca(NO_3)_2$ (0.20 M), and cetylpyridinium chloride (0.02 M) in deionized water (15 mL) sequentially at 40 °C to form a viscous clear calcium source solution with pH adjusted to 8.0 by ammonium hydroxide. The phosphate source solution with pH ~ 8.0 was prepared by dissolving $(NH_4)_2HPO_4$ (0.12 M) in a second container of deionized water (15 mL). The two solutions were mixed together, forming the synthetic solution for the tertiary hydrothermal deposition. The experimental set-up for tertiary hydrothermal growth was the same as for secondary growth except the starting substrate was the film of HAP after secondary growth. The tertiary growth reaction was carried out for 60 h at 200 °C and autogenous pressure. To keep sufficient calcium and phosphate ions for HAP film growth during the reaction, the synthetic solution was replaced with fresh solution after every 15 h.

Product Characterization: The crystal structure of HAP was determined by X-ray powder diffraction (XRD, Philips PW3020) with Cu Kα radiation ($\lambda = 1.5418$ Å). Images of particle morphology and elemental analysis of the products were obtained using a field-emission source scanning electron microscope (FESEM, Zeiss-Leo DSM982) equipped with an EDX spectrometer (EDAX Phoenix). The FTIR spectrum was recorded with a spectrophotometer (FTIR-8400S Shimadzu) in the range of 500–2000 cm^{-1}. Proton conductivity measurements of the membranes were carried out using an impedance spectroscopy (EIS 300, Gamry Instruments) over a frequency range of 300 kHz to 0.1 Hz. The upper surface of the HAP film was sputter-coated with ~300 nm of palladium/gold (60%/40%) alloy as electrode. The electrical platinum leads were attached to both sides of the membrane using platinum paint (SPI Supplies/Structure Probe, Inc.). The membrane was attached to the end of an alumina tube using ceramic adhesive (Ceramabond 569, Aremco Products, Inc.), with the HAP film faced outward. The tube was placed in a tube furnace for temperature control. To avoid palladium embrittlement, nitrogen was fed to the inside of the tube as it was heated. The gas flow was switched to hydrogen when the temperature reached 300 °C. The membrane was heated stepwise with a ramp rate of 2 °C min^{-1}, with the membrane maintained at constant temperature for at least 1 h prior to each conductivity measurement.

Acknowledgements

We acknowledge support from the NSF (CMMI-0856128), DOE (DE-FG02-05ER15722) and the DOE through the Laboratory for Laser Energetics (DE-FC03-92SF19460) for support of this research. Supporting Information is available online from Wiley InterScience or from the author.

Received: February 20, 2009
Revised: August 15, 2009

---

[1] R. M. Ormerod, *Chem. Soc. Rev.* **2003**, *32*, 17.
[2] T. Norby, *Nature* **2001**, *410*, 877.
[3] L. Carrette, K. A. Friedrich, U. Stimming, *ChemPhysChem* **2000**, *1*, 162.
[4] K. A. Mauritz, R. B. Moore, *Chem. Rev.* **2004**, *104*, 4535.
[5] M. A. Hickner, H. Ghassemi, Y. S. Kim, B. R. Einsla, J. E. McGrath, *Chem. Rev.* **2004**, *104*, 4587.
[6] J. B. Goodenough, *Annu. Rev. Mater. Res.* **2003**, *33*, 91.
[7] B. C. H. Steele, A. Heinzel, *Nature* **2001**, *414*, 345.
[8] N. P. Brandon, S. Skinner, B. C. H. Steele, *Annu. Rev. Mater. Res.* **2003**, *33*, 183.
[9] S. M. Haile, D. A. Boysen, C. R. I. Chisholm, R. B. Merle, *Nature* **2001**, *410*, 910.
[10] D. J. L. Brett, A. Atkinson, N. P. Brandon, S. J. Skinner, *Chem. Soc. Rev.* **2008**, *37*, 1568.
[11] Z. Lai, G. Bonilla, I. Diaz, J. G. Nery, K. Sujaoti, M. A. Amat, E. Kokkoli, O. Terasaki, R. W. Thompson, M. Tsapatsis, D. G. Vlachos, *Science* **2003**, *300*, 456.

[12] G. N. Karanikolos, J. W. Wydra, J. A. Stoeger, H. García, A. Corma, M. Tsapatsis, *Chem. Mater.* **2007**, *19*, 792.
[13] K. Yamashita, H. Owada, T. Umegaki, T. Kanazawa, T. Futagami, *Solid State Ionics* **1988**, *28–30*, 660.
[14] T. Kawasaki, *J. Chromatogr.* **1991**, *544*, 147.
[15] G. C. Maiti, F. Freund, *J. Chem. Soc. Dalton Trans.* **1981**, 949.
[16] S. Nakamura, H. Takeda, K. Yamashita, *J. Appl. Phys.* **2001**, *89*, 5386.
[17] K. Yamashita, K. Kitagaki, T. Umegaki, *J. Am. Ceram. Soc.* **1995**, *78*, 1191.
[18] S. Ban, S. Maruno, *J. Biomed. Mater. Res.* **1998**, *42*, 387.
[19] S. Ban, J. Hasegawa, *Biomaterials* **2002**, *23*, 2965.
[20] J. Xie, B. Luan, *J. Mater. Sci. : Mater. Med.* **2008**, *19*, 3211.
[21] K. Govender, D. S. Boyle, P. B. Kenway, P. O'Brien, *J. Mater. Chem.* **2004**, *14*, 2575.
[22] N. Ito, M. Iijima, K. Kimura, S. Iguchi, *J. Power Sources* **2005**, *152*, 200.
[23] S. N. Paglieri, J. D. Way, *Sep. Purif. Methods* **2002**, *31*, 1.
[24] S. Ban, S. Maruno, *Biomaterials* **1998**, *19*, 1245.
[25] R. K. Roeder, G. L. Converse, H. Leng, W. Yue, *J. Am. Ceram. Soc.* **2006**, *89*, 2096.
[26] M. Andrés-Vergés, C. Fernández-González, M. Martínez-Gallego, *J. Eur. Ceram. Soc.* **1998**, *18*, 1245.
[27] W. Suchanek, H. Suda, M. Yashima, M. Kakihana, M. Yoshimura, *J. Mater. Res.* **1995**, *10*, 521.
[28] H. Füredi-Milhofer, S. Sarig, *Prog. Cryst. Growth Charact. Mater.* **1996**, *32*, 45.
[29] M. D. Sikirić, H. Füredi-Milhofer, *Adv. Colloid Interface Sci.* **2006**, *128–130*, 135.
[30] D. Liu, M. Z. Yates, *Langmuir* **2006**, *22*, 5566.
[31] B. O. Fowler, *Inorg. Chem.* **1974**, *13*, 194.
[32] F. Peters, M. Epple, *J. Chem. Soc. Dalton Trans.* **2001**, 3585.
[33] K. Yamashita, H. Owada, T. Umegaki, T. Kanazawa, K. Katayama, *Solid State Ionics* **1990**, *40–41*, 918.
[34] K. D. Kreuer, *Annu. Rev. Mater. Res.* **2003**, *33*, 333.
[35] S. Gallini, M. Hansel, T. Norby, M. T. Colomer, J. R. Jurado, *Solid State Ionics* **2003**, *162–163*, 167.
[36] W. Suksamai, I. S. Metcalfe, *Solid State Ionics* **2007**, *178*, 627.
[37] J. Guan, S. E. Dorris, U. Balachandran, M. Liu, *Solid State Ionics* **1997**, *100*, 45.
[38] S. Gallini, J. R. Jurado, M. T. Colomer, *J. Eur. Ceram. Soc.* **2005**, *25*, 2003.
[39] P. P. Mardilovich, Y. She, Y. H. Ma, *AIChE J.* **1998**, *44*, 310.
[40] Y. H. Ma, P. P. Mardilovich, Y. She, U.S. Patent 6152987, **2000**.